

Biosynthesis of cinchona alkaloids

<https://doi.org/10.1038/s41586-026-10227-x>

Received: 27 October 2025

Accepted: 3 February 2026

Published online: 18 March 2026

Open access

 Check for updates

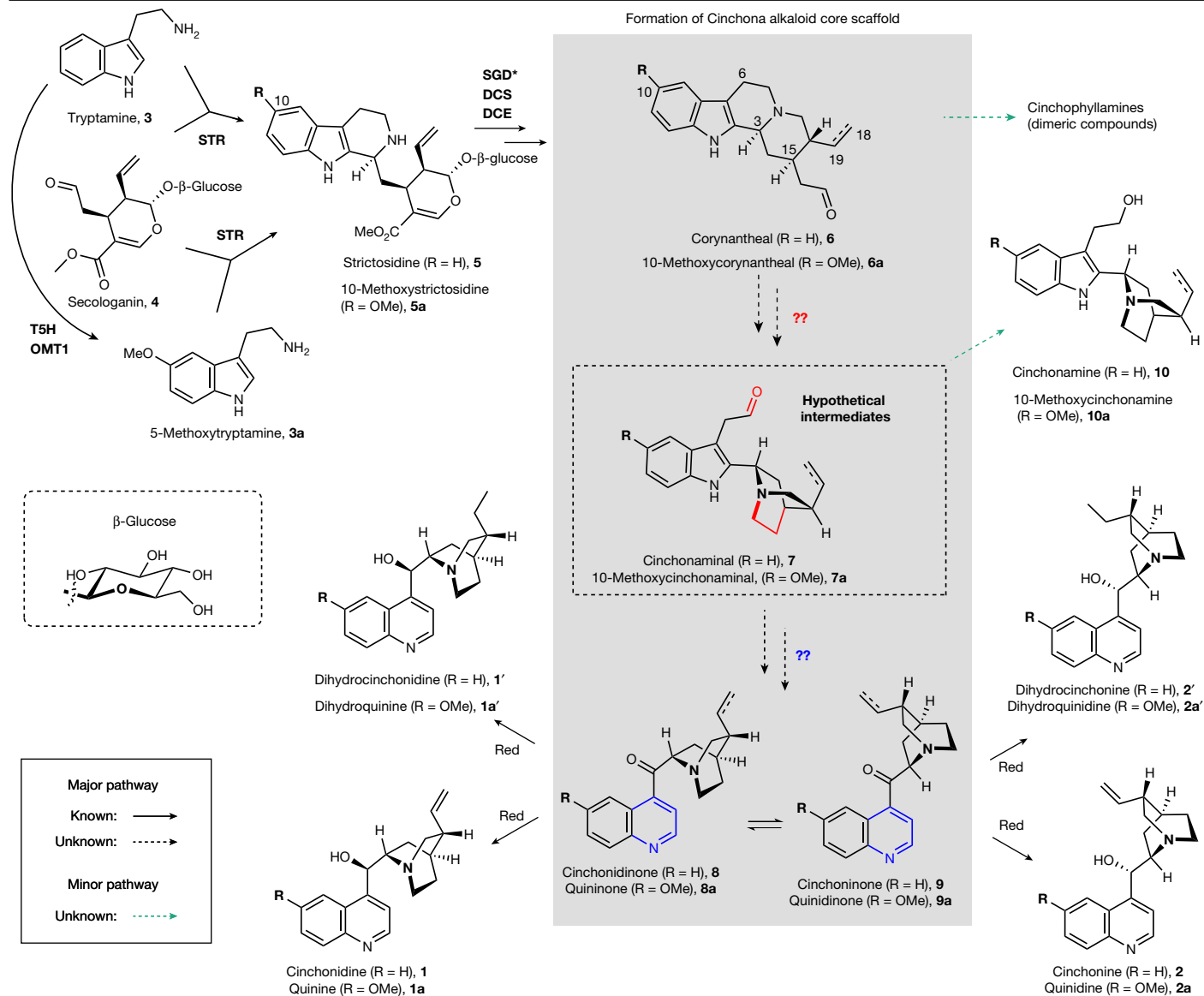
Blaise Kimbadi Lombe^{1,7}, Tingan Zhou^{1,7}, Gyumin Kang¹, Joshua C. Wood², John P. Hamilton^{2,3}, Klaus Gase¹, Yoko Nakamura¹, Ryan M. Alam¹, Ron P. Dirks⁴, Lorenzo Caputi¹, C. Robin Buell^{2,5,6}✉ & Sarah E. O'Connor^{1,8}

Cinchona alkaloids, which have been studied for more than 250 years, are plant-derived natural products that have collectively had a substantial impact in medicine and basic science^{1–5}. Examples of cinchona alkaloids include quinine, a historically important antimalarial drug, and cinchonidine, a chiral catalyst widely used in process chemistry. However, it is still largely unknown how plants synthesize these well-known compounds. Here we report the discovery of genes responsible for the biosynthesis of the distinctive quinoline–quinuclidine scaffold of cinchona alkaloids. A combination of isotopic labelling, gene silencing, single-nucleus RNA sequencing and comparative transcriptomics revealed the involvement of several unexpected biosynthetic transformations. We also describe a previously unreported quaternary amine intermediate that is generated through an unusual enzymatic cyclization. We show that dihydroquinine(di)none, dihydrocinchonine(di)none and cinchonine(di)none can be produced when these genes are heterologously expressed in *Nicotiana benthamiana*. Furthermore, we demonstrate that this *N. benthamiana* expression platform can convert non-native fluorinated and chlorinated tryptamine substrates into dihydrocinchonine(di)none analogues, which suggests that these biosynthetic enzymes can be leveraged to produce halogenated cinchona alkaloid derivatives. These discoveries uncover the long-standing mystery of how the cinchona alkaloid scaffold is biosynthesized and highlight prospects for access to these compounds through metabolic engineering approaches.

Cinchona alkaloids are a group of structurally diverse, nitrogen-containing compounds that are primarily found in *Cinchona* plants. The best known of these alkaloids, quinine (**1a**), is the earliest known naturally occurring treatment for malaria⁶ and is used as a bittering agent in foods and beverages such as tonic water and bitter lemon. Cinchona alkaloids also include quinidine (**2a**), an antiarrhythmic drug that acts through the inhibition of sodium and potassium channels^{7–9}, and the non-methoxylated analogues cinchonidine (**1**) and cinchonine (**2**), which are widely used as chiral catalysts for synthetic chemistry^{10,11}. Dihydro analogues of these alkaloids (dihydrocinchonidine (**1'**), dihydrocinchonine (**2'**), dihydroquinine (**1a'**) and dihydroquinidine (**2a'**), congeners with a single bond at C-18–C-19) are produced in parallel by plants and display comparable properties to **1(a)**–**2(a)**^{11,12}. Cinchona alkaloids have also been the subject of long-standing investigation in the field of organic chemistry^{2,13}. Quinine was isolated in 1820 (ref. 4), subjected to structural characterization in 1908 (ref. 14) and the chemical structure was fully established in the 1940s¹⁵. Unsuccessful attempts to synthesize quinine in the 1850s resulted in a serendipitous discovery of mauve, the world's first synthetic dye^{16–18}. A racemic formal synthesis process was eventually accomplished in 1945 (ref. 19) and a stereoselective total synthetic route was achieved in 2001 (ref. 20). Overall, cinchona alkaloids have had seminal roles in the fields of medicine, organic synthesis and natural product chemistry^{1,2}.

From a biosynthetic perspective, quinine and other cinchona alkaloids are classified as monoterpene indole alkaloids^{12,21}. Monoterpene indole alkaloids are natural products that originate from the enzymatic condensation of tryptamine (**3**, derived from tryptophan²²) and the geraniol-derived monoterpene²³ secologanin (**4**) to form the tetrahydro- β -carboline intermediate strictosidine (**5**)²¹. This reaction is catalysed by the enzyme strictosidine synthase (STR) (note that throughout, protein and gene symbols relate to *Cinchona pubescens* unless otherwise indicated) (Fig. 1 and Supplementary Fig. 1). Strictosidine, after enzymatic deglycosylation, is acted on by a reductase (dihydrocorynantheine aldehyde synthase (DCS)) and an esterase (dihydrocorynantheine aldehyde esterase (DCE)) to form the dihydro congener of corynantheal (dihydrocorynantheal (**6'**))²⁴. Plant feeding studies suggest that both **6'** and corynantheal (**6**) congeners undergo, in parallel, a series of unknown steps to form the hypothetical indole–quinuclidine intermediates cinchonamine (**7**) and dihydrocinchonamine (**7'**)²⁵, which are thought to undergo conversion, again through a series of unknown chemical transformations, to form the quinoline core of **1**, **1'**, **2** and **2'**. Recent work has shown that the methoxy group observed in **1a**, **1a'**, **2a** and **2a'** is introduced onto the starting precursor tryptamine by tryptamine-5-hydroxylase (T5H) and the *O*-methyltransferase OMT1 (ref. 26). Feeding studies have confirmed that the biosynthesis of methoxylated congeners proceeds in the same way as for **1** and **2** via a parallel biosynthetic pathway, with

¹Department of Natural Product Biosynthesis, Max Planck Institute for Chemical Ecology, Jena, Germany. ²Center for Applied Genetic Technologies, University of Georgia, Athens, GA, USA. ³Department of Crop and Soil Sciences, University of Georgia, Athens, GA, USA. ⁴Future Genomics Technologies, Leiden, The Netherlands. ⁵Institute of Plant Breeding, Genetics and Genomics, University of Georgia, Athens, GA, USA. ⁶The Plant Center, University of Georgia, Athens, GA, USA. ⁷These authors contributed equally: Blaise Kimbadi Lombe, Tingan Zhou. ✉e-mail: Robin.Buell@uga.edu; oconnor@ice.mpg.de



precursors. A detailed and updated biosynthetic schematic and a summary of key feeding experiments are given in Supplementary Figs. 1 and 2. The asterisk on SGD indicates that functional characterization of this enzyme is reported here (Supplementary Fig. 3). Red designates previously reported catalytic activity that has been observed in crude samples of *Cinchona* tissues, but the corresponding protein and gene were not reported⁴⁰. For a complete list of compound names, structures and numbers mentioned in this work, see Supplementary Information.

of downstream cinchona alkaloids. To test this hypothesis, we chemically synthesized the isotopically labelled analogue *d*₅-corynantheol (**11b**) and fed it to *C. pubescens* tissues (leaf, stem and root). Liquid chromatography and mass spectrometry (LC–MS) analyses of fed tissues confirmed the formation of both *d*₅-cinchonidine (**1b**) and *d*₅-cinchonine (**2b**), and the indole–quinuclidine *d*₅-cinchonamine (**10b**). This result establishes **11** as an on-pathway intermediate (Fig. 2a–c).

Discovery of additional biosynthetic intermediates

Notably, we also detected efficient isotopic incorporation of **11b** into an unknown metabolite with a pseudomolecular ion at *m/z* 279.1856 (denoted compound **12**) (Fig. 2d and Supplementary Fig. 4). To test whether **12** is also an on-pathway intermediate, we fractionated the isotopically labelled form of this compound from *C. pubescens* tissues that had been fed with **11b**. The fractionated part was then re-fed to fresh *C. pubescens* tissues. Subsequent LC–MS analyses confirmed that this metabolite is a precursor for the alkaloids **1, 2** and

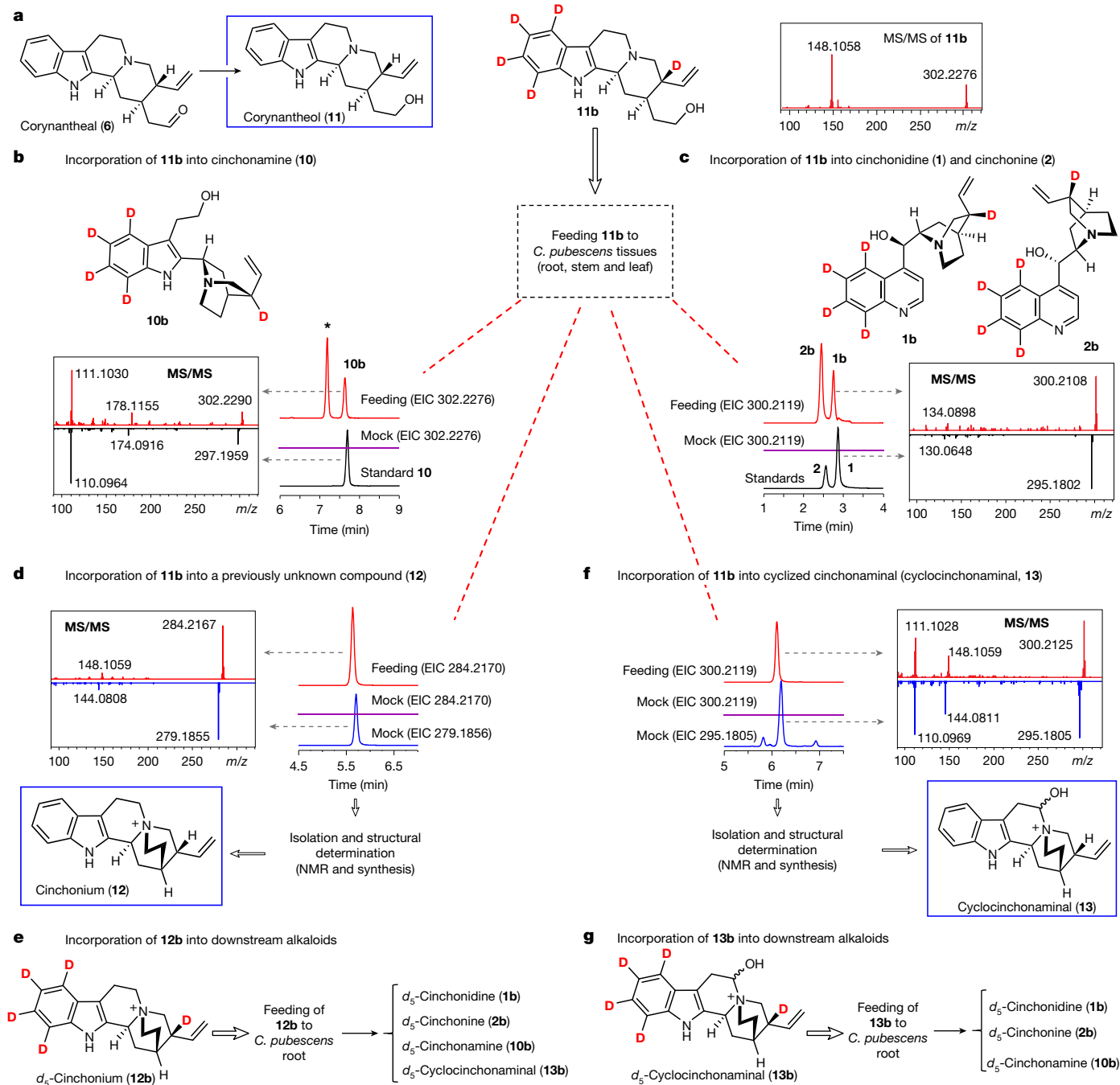


Fig. 2 | Identification of three key on-pathway intermediates (11–13) through feeding studies. **a**, Schematic illustrating the natural conversion of **6** into the corresponding alcohol congener **11**, along with the structure of the synthetic isotopically labelled analogue **11b** that was used to feed tissues from *C. pubescens* plantlets. MS/MS (20 to 50 eV) spectrum of the synthetic subtract **11b** is shown. **b**, **c**, Extracted ion chromatograms (EICs) and MS/MS (20 to 50 eV) spectra evidencing the incorporation of **11b** into **1**, **2** and **10**. Labeled compounds elute slightly faster than the non-labelled counterparts (a retention time difference of about 0.05 min). In **b**, the asterisk indicates an unknown compound that is not part of the cinchona alkaloid pathway as evidenced by re-feeding experiments with partially purified material of that

cinchonamine (**10**) (Fig. 2e, and Supplementary Fig. 5). Large-scale isolation, semi-synthesis and NMR analyses established that this major metabolite is a quaternary ammonium, a scaffold previously unreported in the metabolism of *Cinchona*. Therefore we named **12** as cinchonium (Fig. 2d).

labelled compound. Data showing incorporation of **11b** into keto-quinoline intermediates **8** and **9** are provided in Supplementary Fig. 4. **d–g**, Identification of a previously unknown compound, **12**, and cyclized cinchonamine (**13**) as on-pathway intermediates. EIC and MS/MS spectra evidencing the incorporation of **11b** into **12** and **13** are shown. Details on the structural characterization and synthesis of **12** and **13** are provided in the Supplementary Information. EIC and MS/MS spectra demonstrating the incorporation of **12b** and **13b** into downstream alkaloids **1**, **2**, **10** and **13** are similar to the data shown in **b**, **c** and **f** (Supplementary Fig. 5). Mock denotes samples fed with water instead of the labelled compound (control group).

Feeding of **11b** and d_5 -cinchonium (**12b**) to *C. pubescens* tissues also led to the detection of a native compound with a molecular mass (m/z of 295.1805) and a tandem MS (MS/MS) fragmentation pattern similar to commercially available **10** (an alcohol with an m/z of 297.1961), which suggested that the detected metabolite was the long-predicted²⁵

aldehyde intermediate cinchonamal (Figs. 1 and 2f and Supplementary Fig. 6). As with **12**, an isotope-labelled derivative of this target (putative cinchonamal) was partially purified from fed plant tissues, tested as an intermediate by re-feeding to *C. pubescens* tissues and confirmed by LC–MS analysis to be incorporated into **1** and **2** (Fig. 2g). Isolation, semi-synthesis and NMR and MS/MS analyses confirmed that the target compound is the predicted cinchonamal, but predominantly existing in the hemiaminal cyclized form **13** (herein referred to as cyclocinchonamal; Fig. 2f). To our knowledge, this result marks the first time that this intermediate has been isolated and structurally characterized (Supplementary Fig. 7).

In summary, the identification and incorporation of these three intermediates—**11**, **12** and (cyclo)cinchonamal (**13**)—led us to propose a revised biosynthetic hypothesis. Corynantheol is reduced to **11**, which is then cyclized to form the newly identified quaternary amine **12**. Cinchonium is converted into **7** (or the cyclized form **13**), the first biosynthetic intermediate with the distinctive indole–quinuclidine moiety of cinchona alkaloids. (Cyclo)cinchonamal then undergoes oxidative rearrangement²⁵ to form the quinoline scaffold found in all cinchona alkaloids, followed by reduction of the ketone function to produce the end products **1** and **2**.

Conversion of corynantheol to malonyl-corynantheol

With this revised biosynthetic hypothesis in hand, we set out to identify the reductase responsible for converting **6** to **11**. We mined a RNA sequencing (RNA-seq) dataset from *C. pubescens* and selected eight putative reductases that were co-expressed with DCS (Pearson's coefficient (r) > 0.5; Extended Data Fig. 1a). During reconstruction of the early-stage pathway in *N. benthamiana*, the last known intermediate, **6'**, was observed to undergo reduction to its corresponding alcohol, dihydrocorynantheol (**11'**)²⁶, probably through the action of native reductases in *N. benthamiana*. Therefore, the selected candidates were expressed in *Escherichia coli*, purified and tested in vitro using the enzymatically accessible dihydro analogue of **6'** as the substrate. All tested enzymes (named KR1–KR8) displayed various levels of reductive activity. This result suggests that **6'** can be readily reduced in *C. pubescens* (Extended Data Fig. 1a).

We next investigated how the scaffold **11** is converted to **12**. Model chemistry has shown that **11'** can be converted to dihydrocinchonium (**12'**) via tosylation of the alcohol followed by refluxing^{28,29}. We proposed that biosynthesis in *Cinchona* could proceed in a similar manner if a suitable leaving group is enzymatically installed on the corynantheol scaffold. This leaving group could then be eliminated through intramolecular nucleophilic substitution to generate the quinuclidine ring of **12**. We mined transcriptomic data obtained from *C. pubescens* bulk tissue for genes encoding putative transferases (sulfoltransferases, acyltransferases, kinases and *O*-methyltransferases). A total of 30 candidates that were co-expressed with genes encoding the upstream DCE, DCS and STR enzymes were selected and transiently expressed in *N. benthamiana* leaves, followed by infiltration of **11**. LC–MS analyses of crude extracts of the transformed leaves indicated that only one enzyme, encoded by a putative BAHD-acyltransferase gene^{30,31}, could metabolize **11** to produce a new compound with a mass that corresponded to a malonylated derivative of corynantheol (m/z of 383.197; Extended Data Fig. 1b,c). The same product was observed when the enzyme was assayed in vitro with corynantheol in the presence of malonyl-CoA (Supplementary Fig. 8a,b). MS/MS analysis (Extended Data Fig. 1c) and NMR data (Supplementary Fig. 8c) of the partially purified product established that the produced compound is the *O*-malonylated derivative of corynantheol (**14**, herein referred to as malonyl-corynantheol), thereby confirming that this enzyme is an *O*-malonyltransferase (MAT). Although MAT showed acetyltransferase activity in vitro, this substrate specificity was not observed in *N. benthamiana*, even when acetyl-CoA was exogenously infiltrated along with **11**. This result suggests that this observed

in vitro acetylation is probably due to promiscuous enzyme activity (Supplementary Fig. 8d).

Notably, **14** could not be detected in any *Cinchona* tissues. To validate that **14** is a true pathway intermediate, we attempted to feed enzymatically synthesized isotopically labelled *d*₅-malonyl-corynantheol (**14b**) to *C. pubescens* root tissue. However, NMR analysis in protic solvent (methanol-*d*₃) indicated that **14b** hydrolyses to corynantheol over time (Supplementary Fig. 9). Moreover, LC–MS analysis of *C. pubescens* tissues fed with *d*₅-malonyl-corynantheol revealed the presence of the demalonylated compound (**11b**). Therefore, although we observed isotopically labelled late-stage alkaloids (for example, **2**) in these feeding experiments (Supplementary Fig. 10), we could not unequivocally establish whether it was **11b** or **14b** that was being incorporated. We therefore developed a virus-induced gene silencing (VIGS) assay using in vitro germinated *C. pubescens* plantlets to assess the function of MAT in vivo. After silencing MAT, both congeners **11** and **11'**, and methoxylated analogues, accumulated in high levels in the VIGS-treated *Cinchona* leaves (Extended Data Fig. 1e,f and Supplementary Fig. 11a). Although levels of the downstream alkaloids were not affected after silencing (Supplementary Fig. 11b), presumably because leaves have high levels of the downstream **12** intermediate that would compensate for low levels of the upstream intermediate **11**, the substantial accumulation of corynantheol congeners strongly suggests that MAT acts on these substrates in vivo.

Conversion of malonyl-corynantheol to cinchonium

With the biosynthetic function of MAT established in planta, we set out to identify the enzyme responsible for the proposed unusual cyclization-mediated displacement of malonate that would generate **12** from **14**. A wide range of candidate enzymes, including decarboxylases, esterases, hydrolases and oxidases, were tested in *N. benthamiana*. However, none exhibited detectable catalytic activity on **14**. At this point, annotation-based candidate selection became uninformative. Because a large number of putative biosynthetic genes (>5,000) were co-expressed with MAT in the RNA-seq dataset, we used a combination of approaches to narrow down the number of candidates to be screened. First, we generated a cell-type-resolved transcriptome through single-nucleus RNA sequencing (snRNA-seq) of *C. pubescens* young leaves (Fig. 3a and Supplementary Fig. 12). This dataset revealed a high enrichment of previously identified pathway genes that encode TDC, STR, STTr, DCS and DCE, as well as the newly identified MAT, in three specific clusters (clusters 4, 5 and 6; Fig. 3b). These clusters were putatively assigned as epidermal cells based on their homology to cell markers from the phylogenetically related plant *Catharanthus roseus*³². Second, crude soluble protein extracts obtained from *C. pubescens* root, leaf and leaf apoplastic fluid could cyclize **14** to form **12** (Fig. 3c and Supplementary Fig. 13). These protein extracts were then partially purified using ion exchange and size-exclusion chromatography, and catalytically active fractions were subjected to proteomic analyses. The proteomes of these three samples were then compared with each other and with the available transcriptomic data (Fig. 3c). Third, we noted a previously published report describing the presence of a cinchonium analogue (hydroxylated dihydrocinchonium), ophiorrhizine³³, in *Ophiorrhiza major*, which, like *Cinchona*, is a member of the Rubiaceae family. Feeding the leaves of an available species from the *Ophiorrhiza* genus (*Ophiorrhiza mungos*) with **14b** led to high incorporation into *d*₅-cinchonium (**12b**). This result suggests that the cyclase is conserved in this phylogenetically related plant (Fig. 3d and Supplementary Fig. 14). Notably, feeding *d*₅-malonyl-corynantheol to another Rubiaceae species, *Mitragyna speciosa*, also led to the formation of **12b**, although cinchonium is not normally present in the metabolome of this plant. On the basis of these findings, we generated an *O. mungos* leaf transcriptomic dataset and compared it to available *C. pubescens* and *M. speciosa* transcriptome datasets to identify conserved biosynthetic

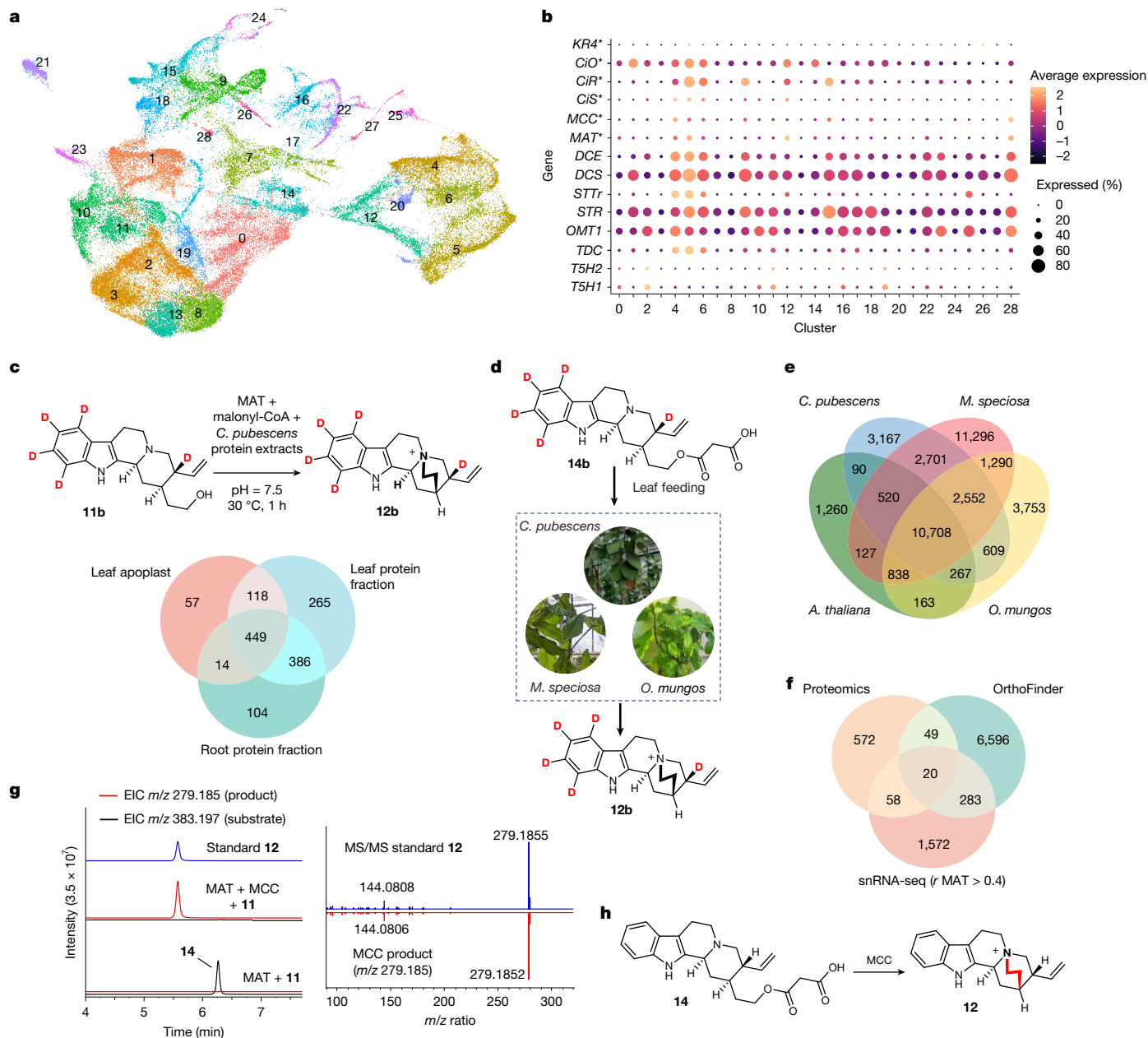


Fig. 3 | Discovery and functional characterization of MCC. **a**, Uniform manifold approximation and projection (UMAP) plot of *C. pubescens* leaf nuclei with high-quality snRNA-seq data, coloured by cell clusters. **b**, Gene expression heatmap of *C. pubescens* known upstream alkaloid biosynthetic genes across cell clusters shown in **a**. Genes marked with an asterisk are reported herein. **c**, Top, schematic showing cyclization activity of protein extracts from *C. pubescens*. Bottom, Venn diagram showing shared peptides among the proteomic fractions from *C. pubescens* that displayed catalytic activity. Assay results with protein extracts are shown in Supplementary Fig. 13. **d**, Detection of cyclization activity of *C. pubescens*, *O. mungos* and *M. speciosa* by feeding isotopically labelled **14b** to leaves. For LC-MS data showing results of incorporation, see Supplementary Fig. 14. **e**, Comparison of cross-species

transcriptomes using the OrthoFinder algorithm (with *A. thaliana* included in the analysis to exclude broadly conserved plant genes). The numbers shown in the diagram are numbers of orthologue clusters. **f**, Integration of proteomics, cross-species transcriptomic comparison and leaf snRNA-seq data to refine candidate gene selection. The numbers shown in the diagram are numbers of genes. **g**, Transient expression of *MAT* alone and with *MCC* in *N. benthamiana* along with co-infiltration of **11**. Left, EICs for **14** (m/z 383.197 \pm 0.05 Da [M+H]⁺, black) and for **12** (m/z 279.185 \pm 0.05 Da, red). Chromatogram of the standard **12** is also shown (blue). This experiment was repeated three times with similar results. Right, MS/MS (20–50 eV) spectra of the standard **12** and the MCC product (m/z 279.1852 Da). **h**, Schematic of the reaction catalysed by MCC.

genes^{34,35}. *Arabidopsis thaliana*, which did not show cyclization activity and is phylogenetically distant to the three other plant species (Supplementary Figs. 14 and 15), was included in this analysis to exclude broadly conserved plant genes (Fig. 3e).

By integrating data from snRNA-seq (genes coexpressed with *MAT*, $r > 0.4$), proteomics (shared peptides among all three *C. pubescens* protein fractions) and transcriptomic cross-species comparison

(orthologous genes present in *C. pubescens*, *O. mungos* and *M. speciosa* but absent in *A. thaliana*), we compiled a list of 20 candidate genes (Fig. 3f). We expressed *MAT* and all these candidates together in *N. benthamiana*. Infiltration of **11** and subsequent LC-MS analyses revealed the formation of **12**. Unexpectedly, deconvolution of the enzyme candidates traced the cyclization activity to a gene annotated as a BAHD malonyltransferase, which we thereafter named

malonyl-corynantheol cyclase (MCC) (Fig. 3g,h). Transiently knocking down the MCC-encoding gene in *C. pubescens* plantlets using VIGS led to an accumulation of **14** and related dihydro and methoxylated congeners. This result confirmed the function of this cyclase in vivo (Supplementary Fig. 16a). In vitro assays showed that MCC did not require cofactors for catalysis and exhibited strict substrate specificity, accepting only malonylated, but not acetylated, corynantheol (Supplementary Fig. 16b). Notably, although both MCC and MAT belong to the BAHD acyltransferase family, these two enzymes do not share high sequence similarity (19.5%) and are phylogenetically distant. MAT clusters with other known BAHD acyltransferases involved in monoterpene indole alkaloid biosynthesis, whereas MCC appears in an evolutionary distant clade (Supplementary Fig. 17). Moreover, MCC did not show malonylation activity and could not install the malonyl group on **11** required for subsequent cyclization to **12** (Supplementary Fig. 18). A potential explanation for the loss of this loss of acyl transferase activity is that its binding pocket for the malonyl-CoA substrate has been extensively mutagenized (Supplementary Fig. 19). A homology model indicates the presence of a binding pocket deeper in the active site. This could conformationally orient **14** such that the nucleophilic amine is proximal to the electrophilic carbon, and the alkyl-chain-bearing malonyl group is in the axial conformation, which would lead to the observed product stereochemistry (Supplementary Fig. 20). The discovery of MAT and MCC as key enzymes that mediate malonylation and subsequent demalonylative cyclization reveals a previously unknown biosynthetic strategy to form this quaternary amine and broadens the functional range of BAHD acyltransferases beyond canonical acyl transfer reactions³⁶.

Conversion of cinchonium to quinoline alkaloids

We then set out to find the gene responsible for the conversion of **12** to the next known biosynthetic intermediate cinchonaminal **7**. Hydroxylation of cinchonium would directly produce **13**, the cyclic form of **7**. Therefore, we searched for biosynthetic genes predicted to encode oxidases. All annotated cytochrome P450 enzymes and oxoglutarate-dependent dioxygenases were ranked on the basis of Pearson's correlation coefficients with MCC using the snRNA-seq data (Extended Data Fig. 2a). A candidate annotated as a 2-oxoglutarate-dependent dioxygenase was confirmed to catalyse this transformation in both *N. benthamiana* and in vitro enzymatic assays, and was subsequently designated as cinchonaminal synthase (CiS) (peak A, Extended Data Fig. 2b,c and Supplementary Fig. 21a). Notably, CiS further oxidized cinchonaminal to form a compound with spectral data consistent with the carboxylic acid (herein named as cinchonaminic acid (**15**); peak B, Extended Data Fig. 2b–d). This compound was not observed in *Cinchona*, which indicated that the next pathway intermediate rapidly intercepts the initial enzymatic product before overoxidation can occur. Conversely, however, *Cinchona* is postulated to reduce **7** to form cinchonamine **10** (Fig. 1). Screening of candidate reductases, obtained through coexpression correlation with CiS (Supplementary Fig. 21b), led to the identification of an alcohol dehydrogenase that converts **7** to **10**, which we named cinchonaminal reductase (CiR) (peak C, Extended Data Fig. 2e–g). CiS and CiR were also enriched in the same clusters (clusters 4–6; Fig. 3b) as the upstream biosynthetic genes (for example, *MAT* and *MCC*) according to the snRNA-seq data. This result suggests that cell-type localization is maintained in these downstream pathway steps.

Conversion of cinchonaminal **7** into a quinoline moiety probably involves oxidative opening of the indole, followed by cyclization and dehydration to form the quinoline scaffold. As the phylogenetically related plant *M. speciosa* uses a cytochrome P450 enzyme (family CYP71) to oxidize an indole to a spirooxindole^{35,37}, we speculated that a *Cinchona* CYP71 P450 enzyme might also be involved in the oxidative transformation of this indole substrate. Because the feeding studies and metabolite accumulation levels indicated that these late-stage steps were more

highly expressed in root and stem tissues (Supplementary Figs. 4 and 22–27), we performed a clustering analysis to prioritize gene candidates based on this expression pattern (Supplementary Fig. 28). Among the top CYP71 P450 candidates selected on the basis of the coexpression analysis with CiS, a functional enzyme was identified, which we named cinchonaminal oxidase (CiO) (Extended Data Fig. 3a,b). CiO catalysed the oxidation of **7**, which produced the two ketone quinoline isomers cinchonidinone (**8**) and cinchoninone (**9**). These stereoisomers, which are known to exist in equilibrium^{38,39}, were observed in a 1:0.23 ratio, which is approximately the same ratio observed in *C. pubescens*. The enzymatic activity of CiO was further confirmed through in vitro assays using yeast microsomes (Supplementary Fig. 29), which demonstrated that this single P450 enzyme can catalyse the indole-to-quinoline ring expansion. VIGS of CiO was also conducted in *C. pubescens*. Leaves in which CiO was silenced showed a significant accumulation of **13** and **10** along with decreased biosynthesis of both ketone quinoline alkaloid stereoisomers (**8** and **9**). This result provides evidence for the physiological function of CiO in planta (Extended Data Fig. 3c–e).

The final step in cinchona alkaloid biosynthesis involves the reduction of the ketone moiety that is generated after the formation of the quinoline scaffold. Previous studies have suggested that this transformation is probably catalysed by a NADPH-dependent oxidoreductase⁴⁰. A total of 60 NADPH-dependent reductase genes that were coexpressed with CiO in the bulk transcriptomic dataset and/or snRNA-seq were cloned and tested (Supplementary Dataset 1). Screening in *N. benthamiana* did not lead to an active candidate. Therefore, we prioritized the selected candidate genes on the basis of the analysis of expression trends (Supplementary Fig. 28a–c) and re-expressed 15 putative aldo-keto reductases and alcohol dehydrogenases (including the above mentioned KR1–KR8) in *E. coli* for assays in vitro. Only one enzyme, KR4, displayed clear reductase activity, converting both non-methoxylated and methoxylated quinoline ketone stereoisomers into the corresponding alcohols (Extended Data Fig. 4a,b). This functional enzyme also reduced the aldehyde function of corynantheal scaffolds (Extended Data Fig. 1a), a result that further supported its involvement in the biosynthesis of cinchona alkaloids. Notably, despite robust activity in vitro, KR4 did not show detectable activity when assayed in *N. benthamiana* leaves after transient expression and infiltration of quinoline ketones. We designed a fusion protein comprising CiO and KR4 for transient expression in *N. benthamiana*. Although oxidation activity of CiO was observed, no reduced product was obtained. To test whether *N. benthamiana* contained endogenous components that inhibit this aldo-keto reductase, diluted crude extracts from *N. benthamiana* leaves were added to in vitro reactions, substituting 10% of the reaction volume. The addition of *N. benthamiana* extract abolished KR4 activity in vitro, a result that implicates the presence of an unknown inhibitory factor that suppresses KR4 function (Extended Data Fig. 4a,b and Supplementary Fig. 30a,b). These results provide a reasonable explanation for the lack of detectable activity in *N. benthamiana* and highlights a potential limitation in using this heterologous system for functional validation of reductases.

Although the two late-stage genes *CiO* and *KR4* were selectively and highly expressed in stem and root tissues, these genes also showed clear enrichment in clusters 4–6 of the leaf snRNA-seq dataset, clusters previously associated with nearly all upstream alkaloid biosynthetic genes (Fig. 3b). Notably, the expression of monoterpene indole alkaloid pathway genes in the Apocynaceae species *C. roseus* seems to switch from epidermal cells to specialized idioblast cells in the late stages of alkaloid biosynthesis³². By contrast, in *Cinchona*, a member of the Rubiaceae family, all alkaloid biosynthetic genes identified in this study were selectively enriched in epidermal cells (clusters 4–6). This consistent cell-type-specific expression pattern of the biosynthetic genes in *Cinchona*, along with high coexpression in bulk tissue (Supplementary Fig. 31), provides further support that these newly identified genes function in the same metabolic pathway and contribute to

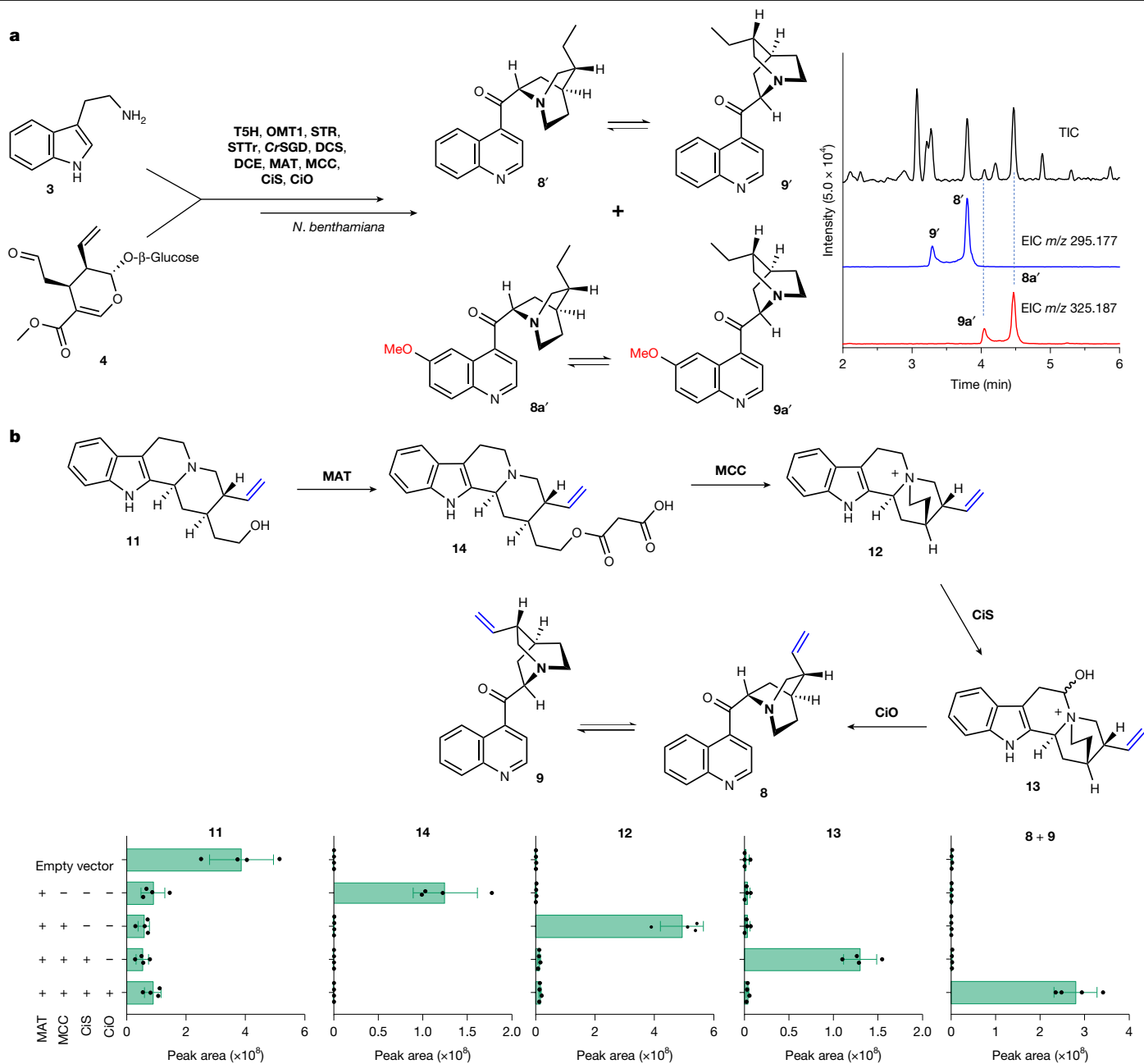


Fig. 4 | Biosynthesis of quinoline cinchona alkaloids. **a**, Production of both methoxylated and non-methoxylated cinchona alkaloids in *N. benthamiana* following transient expression of the indicated biosynthetic enzymes and co-infiltration of **3** and **4**. TIC, total ion chromatogram. **b**, LC-MS peak areas

of products detected in *N. benthamiana* following transient expression (+) or not (-) of the indicated biosynthetic enzymes from *C. pubescens* and incubation with **11** using a leaf-disc assay. Data are the mean \pm s.d. ($n = 4$ biological replicates).

the biosynthesis of cinchona alkaloids. However, we note that KR4 did not exhibit absolute stereoselectivity with the ketone quinoline alkaloids (**8**, **9**, **8a** and **9a**). In particular, with the methoxylated analogues **8a**–**9a**, a stereoisomer that is not observed in the plant was formed in higher levels than the naturally observed stereoisomers (Supplementary Fig. 30c,d). Although this reductase showed clear activity with the quinolines, it is possible that a reductase with higher stereoselectivity remains to be identified.

Reconstitution of natural and unnatural alkaloids

With these enzymes identified and functionally characterized, the cinchona alkaloid biosynthetic pathway could be reconstituted in the heterologous host *N. benthamiana*. The well-known central

monoterpene indole alkaloid precursor **5** was externally supplied as a substrate to discs taken from *N. benthamiana* leaves that had been transformed with DCS, DCE, MAT, MCC, CiS and CiO, along with a construct encoding strictosidine β -glucosidase (SGD) from the phylogenetically related plant *C. roseus* (*CrSGD*), an orthologue of SGD with high catalytic activity (Supplementary Fig. 3). No corynantheal reductase gene was included because the endogenous *N. benthamiana* enzymes efficiently reduced (dihydro)corynantheal. As anticipated, strictosidine was efficiently converted to **8'** and **9'** (Extended Data Fig. 5 and Supplementary Figs. 32 and 33). Reconstruction with the methoxylated analogue 10-OMe strictosidine (**5a**) instead led to the formation of **8a'** and **9a'**. This result confirms the substrate flexibility of the downstream enzymes and provides clear experimental support for the parallel biosynthetic route previously proposed for methoxylated

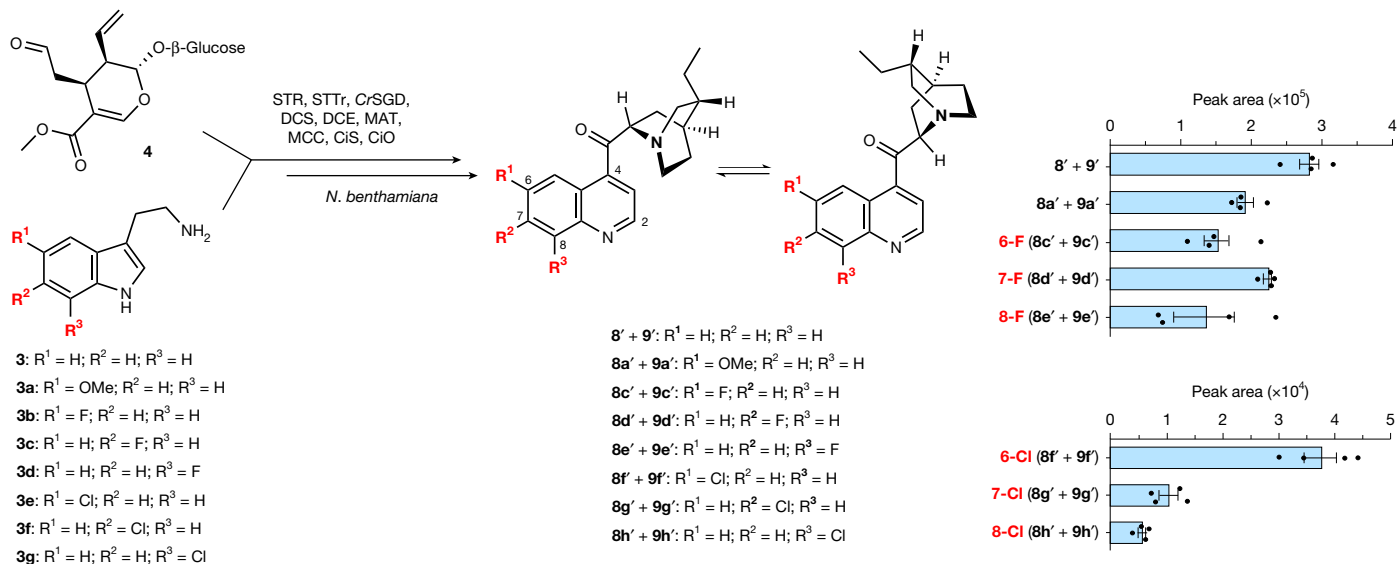


Fig. 5 | Biosynthesis of halogenated analogues of quinoline cinchona alkaloids. Directed biosynthesis of fluorinated and chlorinated analogues of cinchona alkaloids in *N. benthamiana* following transient expression of the indicated biosynthetic enzymes and co-infiltration of **4** and halogenated

alkaloids²⁶ (Extended Data Fig. 5). Notably, the addition of STR, T5H, OMT1 and the vacuolar strictosidine transporter²⁶ STTr to the gene stack, along with replacement of **5** with **3** and **4**, led to the formation of a mixture of methoxylated and non-methoxylated keto quinolines (**8'**, **9'**, **8a'** and **9a'**), which mimicked the occurrence of these dihydro alkaloids in *Cinchona* (Fig. 4a and Supplementary Fig. 34). Because under these assay conditions, DCS leads to **6'**, we tested synthetic **11** as an exogenous substrate for *N. benthamiana* leaf discs (transformed with MAT, MCC, CiS and CiO) to observe the formation of **8** and **9** (Fig. 4b). Moreover, intermediates that we had identified at the outset of this study—**11**, **12** and **13**—were detected when these transformed *N. benthamiana* leaves were subjected to analysis. By contrast, **14** was undetectable when enzymes downstream of MAT (MCC, CiS and CiO) were present, a result consistent with the absence of this transient intermediate in native *C. pubescens* metabolite profiles (Fig. 4b). Collectively, these findings highlight the potential for the biosynthetic production of medicinally relevant quinoline alkaloids using these biosynthetic genes.

Directed biosynthesis, in which the host generating the product is supplied with an exogenous unnatural starting substrate, is a method that has been used for decades to produce industrially important natural product analogues^{34,41–45}. However, for successful production of end-product analogues, this approach requires that all of the downstream enzymes catalyse conversion of all corresponding unnatural biosynthetic intermediates. As *Cinchona* biosynthetic enzymes naturally act on both methoxy and dihydro derivatives, we rationalized that these biosynthetic enzymes would be well suited for the production of unnatural alkaloid analogues. Transformed *N. benthamiana* leaves (STR, CrSGD, DCS, DCE, MAT, MCC, CiS and CiO) were infiltrated with a series of analogues of **3** (5-fluorotryptamine, 5-chlorotryptamine, 6-fluorotryptamine, 6-chlorotryptamine, 7-fluorotryptamine and 7-chlorotryptamine), along with the natural co-substrate **4**. In all cases, we saw consumption of the halogenated tryptamine substrate, along with the presence of compounds with a mass and MS/MS pattern consistent with the formation of the corresponding dihydrocinchonine and dihydrocinchonidine analogues (Fig. 5 and Supplementary Figs. 35 and 36). These results suggest that the identified biosynthetic genes can be used to produce halogenated cinchona alkaloid analogues, which will be potentially useful for medicinal chemistry

tryptamines (**3b–3g**). LC-MS peak areas are shown and data are the mean \pm s.e.m. ($n = 4$ biological replicates). Data from assays using the native substrates, **3** and **3a**, are included for relative comparison of the efficiency of the enzymes. For EICs and MS/MS data, see Supplementary Figs. 35 and 36.

applications given the clinical use and attractiveness of halogenated quinolines⁴⁶.

Conclusion

Here we described the genetic basis that underlies the biosynthesis of the quinoline–quinuclidine scaffold that characterizes cinchona alkaloids. Although aspects of the biosynthesis, such as the mechanism underlying the formation of the C-18–C-19 double bond, remain to be resolved, the discovery of these genes enables biosynthetic conversion from known starting materials to (dihydro)cinchoni(di)ne and (dihydro)quini(di)ne. These discoveries were achieved by integrating modern omics approaches—namely single nucleus sequencing and comparative transcriptomics—along with classical methods of isotopic feeding and enzyme activity fractionation from plant tissues, and the development of a functional in planta assay using VIGS. We demonstrated how simultaneous application of these approaches can substantially streamline the list of gene candidates to be screened. We further demonstrated the application of these biosynthetic genes for the production of natural cinchona alkaloids and non-natural halogenated alkaloid analogues in a *N. benthamiana* host. These discoveries reveal how the distinctive cinchona alkaloid scaffold is biosynthesized and highlights prospects for the metabolic engineering of these complex bioactive alkaloids.

Online content

Any methods, additional references, Nature Portfolio reporting summaries, source data, extended data, supplementary information, acknowledgements, peer review information; details of author contributions and competing interests; and statements of data and code availability are available at <https://doi.org/10.1038/s41586-026-10227-x>.

- Kacprzak, K. M. in *Natural Products: Phytochemistry, Botany and Metabolism of Alkaloids, Phenolics and Terpenes* (eds Ramawat, K. G. & Mérillon, J.-M.) 605–641 (Springer, 2013).
- Kaufman, T. S. & Rúveda, E. A. The quest for quinine: those who won the battles and those who won the war. *Angew. Chem. Int. Ed.* **44**, 854–885 (2005).
- Markham, C. R. S. *Peruvian Bark: A Popular Account of the Introduction of Cinchona Cultivation into British India* (John Murray London, 1880).

4. Pelletier, P. J. & Caventou, J.-B. Recherches chimiques sur les quinquinas. *Ann. Chim. Phys.* **15**, 289–365 (1820).
5. Greenwood, D. The quinine connection. *J. Antimicrob. Chemother.* **30**, 417–427 (1992).
6. Achan, J. et al. Quinine, an old anti-malarial drug in a modern world: role in the treatment of malaria. *Malar. J.* **10**, 144 (2011).
7. Vitali Serdoz, L., Rittger, H., Furlanello, F. & Bastian, D. Quinidine—a legacy within the modern era of antiarrhythmic therapy. *Pharmacol. Res.* **144**, 257–263 (2019).
8. Kehl, S. J. Quinidine-induced inhibition of the fast transient outward K⁺ current in rat melanotrophs. *Br. J. Pharmacol.* **103**, 1807–1813 (1991).
9. Roden, D. M. & Woosley, R. L. Class I antiarrhythmic agents: quinidine, procainamide and N-acetylprocainamide, disopyramide. *Pharmacol. Ther.* **23**, 179–191 (1983).
10. Song, C. E. in *Cinchona Alkaloids in Synthesis and Catalysis* (ed. Song, C. E.) 1–10 (Wiley, 2009).
11. Tian, S.-K. et al. Asymmetric organic catalysis with modified cinchona alkaloids. *Acc. Chem. Res.* **37**, 621–631 (2004).
12. Verpoorte, R., Schripsema, J. & van der Leer, T. in *The Alkaloids: Chemistry and Pharmacology* Vol. 34 (ed. Brossi, A.) 331–398 (Academic Press, 1989).
13. Weinreb, S. M. Synthetic lessons from quinine. *Nature* **411**, 429–431 (2001).
14. Rabe, P. Zur kenntnis der China-alkaloide. VIII. Mitteilung: über die konstitution des cinchonins. *Ber. Dtsch. Chem. Ges.* **41**, 62–70 (1908).
15. Prelog, V. & Zlátný, E. Über China-alkaloide. (6. Mitteilung). Über die konfiguration von (-)-3-methyl-4-äthyl-hexan. *Helv. Chim. Acta* **27**, 545–547 (1944).
16. Perkin, W. H. L. X. I. V. On mauveine and allied colouring matters. *J. Chem. Soc. Trans.* **35**, 717–732 (1879).
17. Perkin, W. H. XIX. On colouring matters derived from coal tar. *Q. J. Chem. Soc. Lond.* **14**, 230–255 (1862).
18. Alegbe, E. O. & Uthman, T. O. A review of history, properties, classification, applications and challenges of natural and synthetic dyes. *Heliyon* **10**, e33646 (2024).
19. Woodward, R. B. & Doering, W. E. The total synthesis of quinine. *J. Am. Chem. Soc.* **66**, 849–849 (1944).
20. Stork, G. et al. The first stereoselective total synthesis of quinine. *J. Am. Chem. Soc.* **123**, 3239–3242 (2001).
21. O'Connor, S. E. & Maresh, J. J. Chemistry and biology of monoterpene indole alkaloid biosynthesis. *Nat. Prod. Rep.* **23**, 532–547 (2006).
22. Kowanko, N. & Leete, E. Biosynthesis of the cinchona alkaloids. I. The incorporation of tryptophan into quinine. *J. Am. Chem. Soc.* **84**, 4919–4921 (1962).
23. Leete, E. & Wemple, J. N. Biosynthesis of the cinchona alkaloids. The incorporation of geraniol-3-¹⁴C into quinine. *J. Am. Chem. Soc.* **88**, 4743–4744 (1966).
24. Trenti, F. et al. Early and late steps of quinine biosynthesis. *Org. Lett.* **23**, 1793–1797 (2021).
25. Battersby, A. R. & Parry, R. J. Biosynthesis of the *Cinchona* alkaloids: late stages of the pathway. *J. Chem. Soc.* <https://doi.org/10.1039/C29710000031> (1971).
26. Lombe, B. K., Zhou, T., Caputi, L., Ploss, K. & O'Connor, S. E. Biosynthetic origin of the methoxy group in quinine and related alkaloids. *Angew. Chem. Int. Ed.* **64**, e202418306 (2025).
27. Verpoorte, R. et al. in *Plant Vacuoles* (ed. Marin, B.) 485–494 (Springer, 1987).
28. Vamvacas, C., Philipsborn, W. V., Schlittler, E., Schmid, H. & Karrer, P. Über die konstitution des melinonins B. 26. Mitteilung über calebassen-alkaloide. *Helv. Chim. Acta* **40**, 1793–1808 (1957).
29. Wenkert, E. & Bringi, N. V. The absolute configuration of some indole alkaloids. *J. Am. Chem. Soc.* **80**, 3484–3484 (1958).
30. Liu, X. et al. Molecular characterization and structure basis of a malonyltransferase with both substrate promiscuity and catalytic regioselectivity from *Cistanche tubulosa*. *Acta Pharm. Sin. B* **14**, 2333–2348 (2024).
31. Unno, H. et al. Structural and mutational studies of anthocyanin malonyltransferases establish the features of BAHD enzyme catalysis. *J. Biol. Chem.* **282**, 15812–15822 (2007).
32. Li, C. et al. Single-cell multi-omics in the medicinal plant *Catharanthus roseus*. *Nat. Chem. Biol.* **19**, 1031–1041 (2023).
33. Arbain, D. et al. Ophiorrhizine, a new quaternary indole alkaloid related to cinchonamine, from *Ophiorrhiza major* Ridl. *J. Chem. Soc. Perkin Trans. 1* <https://doi.org/10.1039/P19920000663> (1992).
34. Schotte, C. et al. Directed biosynthesis of mitragynine stereoisomers. *J. Am. Chem. Soc.* **145**, 4957–4963 (2023).
35. McDonald, A. et al. Enzymatic epimerization of monoterpene indole alkaloids in kratom. *Nat. Chem. Biol.* **22**, 229–238 (2026).
36. Moghe, G. et al. BAHD company: the ever-expanding roles of the BAHD acyltransferase gene family in plants. *Annu. Rev. Plant Biol.* **74**, 165–194 (2023).
37. Nguyen, T.-A. M. et al. Discovery of a cytochrome P450 enzyme catalyzing the formation of spirooxindole alkaloid scaffold. *Front. Plant Sci.* <https://doi.org/10.3389/fpls.2023.1125158> (2023).
38. Rabe, P. Zur kenntnis der chinaalkaloide XII. *Justus Liebigs Ann. Chem.* **373**, 85–120 (1910).
39. Robins, R. J. & Rhodes, M. J. C. An evaluation of the tautomerism of cinchoninone and quinidinone made using a combination of ¹H NMR and ¹³C NMR spectroscopy. *Phytochemistry* **26**, 551–556 (1987).
40. Isaac, J. E., Robins, R. J. & Rhodes, M. J. C. Cinchoninone: NADPH oxidoreductases I and II—novel enzymes in the biosynthesis of quinoline alkaloids in *Cinchona ledgeriana*. *Phytochemistry* **26**, 393–399 (1987).
41. Thiericke, R. & Rohr, J. Biological variation of microbial metabolites by precursor-directed biosynthesis. *Nat. Prod. Rep.* **10**, 265–289 (1993).
42. Seshadri, K. et al. Synthetic biology in natural product biosynthesis. *Chem. Rev.* **125**, 3814–3931 (2025).
43. McCoy, E. & O'Connor, S. E. Directed biosynthesis of alkaloid analogs in the medicinal plant *Catharanthus roseus*. *J. Am. Chem. Soc.* **128**, 14276–14277 (2006).
44. Boccia, M., Grzech, D., Lopes, A. A., O'Connor, S. E. & Caputi, L. Directed biosynthesis of new to nature alkaloids in a heterologous *Nicotiana benthamiana* expression host. *Front. Plant Sci.* <https://doi.org/10.3389/fpls.2022.919443> (2022).
45. Bradley, S. A. et al. Biosynthesis of natural and halogenated plant monoterpene indole alkaloids in yeast. *Nat. Chem. Biol.* **19**, 1551–1560 (2023).
46. Matada, B. S., Pattanashettar, R. & Yernale, N. G. A comprehensive review on the biological interest of quinoline and its derivatives. *Bioorg. Med. Chem.* **32**, 115973 (2021).

Publisher's note Springer Nature remains neutral with regard to jurisdictional claims in published maps and institutional affiliations.



Open Access This article is licensed under a Creative Commons Attribution 4.0 International License, which permits use, sharing, adaptation, distribution and reproduction in any medium or format, as long as you give appropriate credit to the original author(s) and the source, provide a link to the Creative Commons licence, and indicate if changes were made. The images or other third party material in this article are included in the article's Creative Commons licence, unless indicated otherwise in a credit line to the material. If material is not included in the article's Creative Commons licence and your intended use is not permitted by statutory regulation or exceeds the permitted use, you will need to obtain permission directly from the copyright holder. To view a copy of this licence, visit <http://creativecommons.org/licenses/by/4.0/>.

© The Author(s) 2026

Reporting summary

Further information on research design is available in the Nature Portfolio Reporting Summary linked to this article.

Data availability

Data supporting the findings of this work are available within this paper and its Supplementary Information. Sequences of reported genes are included in the Supplementary Information and have been deposited into the National Center for Biotechnology (NCBI) GenBank under the following accession numbers: *MAT* (PX842829), *MCC* (PX842830), *CiS* (PX842831), *CiR* (PX842832), *CiO* (PX842833), *SGD1* (PX842834), *SGD2* (PX842835), *SGD3* (PX842836), *KR1* (PX842837), *KR2* (PX842838), *KR3* (PX842839), *KR4* (PX842840), *KR5* (PX842841), *KR6* (PX842842), *KR7* (PX842843) and *KR8* (PX842844). *C. pubescens* bulk RNA-seq and snRNA-seq, ONT full-length cDNA and ONT gDNA reads have been deposited into the NCBI under BioProject PRJNA1347772. Raw reads from RNA-seq of *O. mungos* leaves have been deposited into the NCBI (accession PRJNA1413194). Bulk RNA-seq of *M. speciosa* from a previous study was downloaded from the NCBI (accession PRJNA1244102) and the transcriptome of *A. thaliana* used is implemented and available in OrthoVenn3 (<https://orthovenn3.bioinfotoolkits.net>). Proteomic data have been deposited into the ProteomeXchange Consortium (dataset identifier PXD068683). Source data are provided with this paper.

Acknowledgements We acknowledge K. Ploß for plant culture cultivation; E. Rothe for plant cultivation; J. Wurlitzer for technical assistance; M. Kunert and S. Heinecke for assistance with MS; F. Trenti for isolation of *C. pubescens* DNA; and B. Vaillancourt for assistance with management of the sequencing data. We acknowledge NIH (AT012783-02) for funding. The plant and tissue art in Extended Data Figs. 1d and 2g were created in BioRender; Lombe, B. <https://biorender.com/8hz4n59> (2025) (agreement number OA2956EHDC).

Author contributions B.K.L., T.Z., S.E.O. and C.R.B. conceived the study and wrote the manuscript. B.K.L. and T.Z. performed feeding experiments, bioinformatic analyses of datasets, identification of gene candidates, isolation of compounds, and in vitro and in planta assays of enzymes. G.K. synthesized compounds and provided key mechanistic insights. J.C.W. performed the snRNA-seq experiments. J.C.W. and J.P.H. processed the snRNA-seq data. B.K.L. and Y.N. performed NMR analyses. B.K.L. and K.G. conducted the VIGS experiments. R.M.A. provided early access to cinchonamine. R.P.D. performed *C. pubescens* genome sequencing. J.C.W., J.P.H. and R.P.D. conducted genome assembly and annotation. L.C. assisted with protein purification and analyses. S.E.O. and C.R.B. raised funds and coordinated the study.

Funding Open access funding provided by Max Planck Society.

Competing interests The authors declare no competing interests.

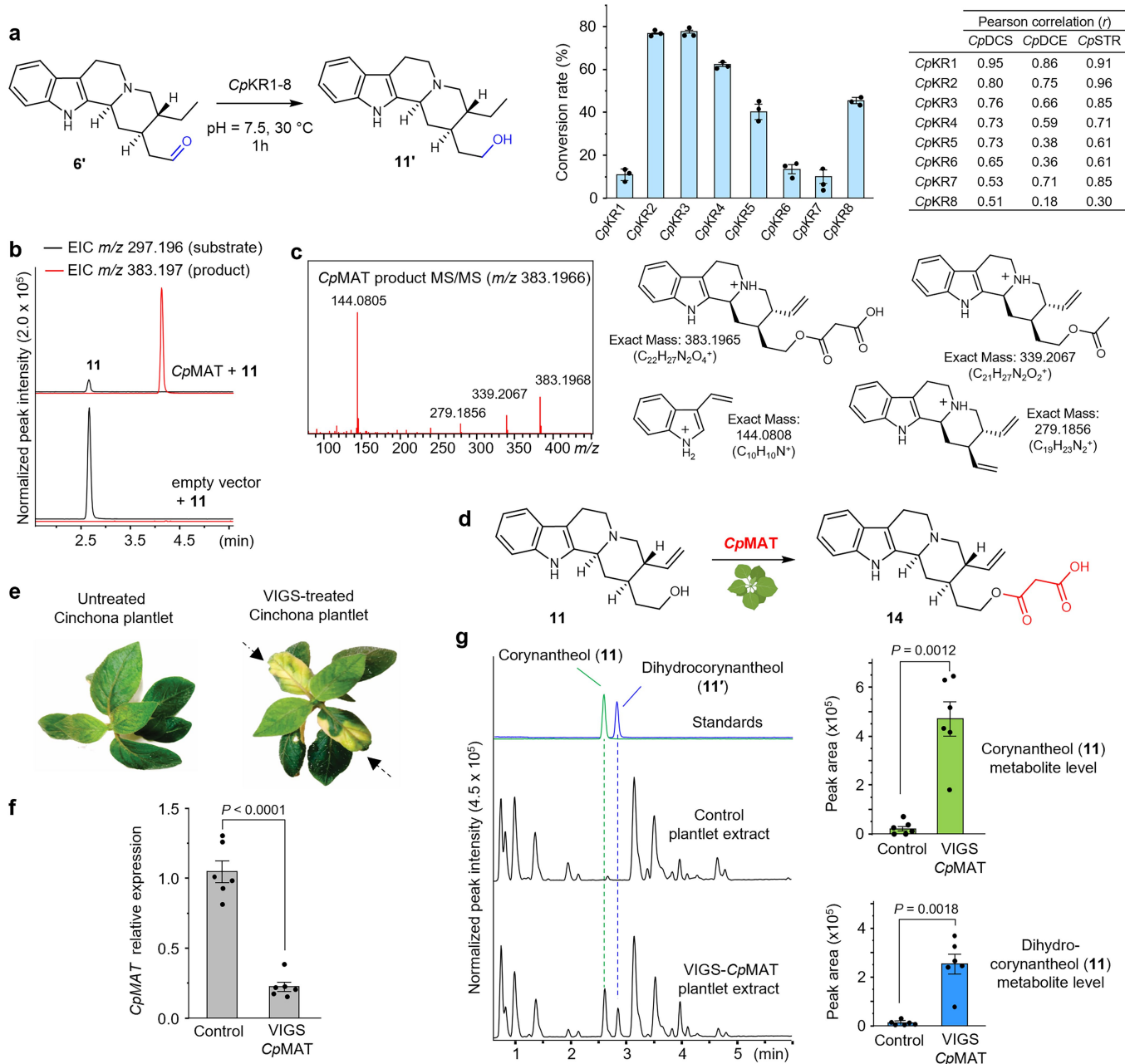
Additional information

Supplementary information The online version contains supplementary material available at <https://doi.org/10.1038/s41586-026-10227-x>.

Correspondence and requests for materials should be addressed to C. Robin Buell or Sarah E. O'Connor.

Peer review information Nature thanks Yanran Li, Shanhui Xu and the other, anonymous, reviewer(s) for their contribution to the peer review of this work. Peer reviewer reports are available.

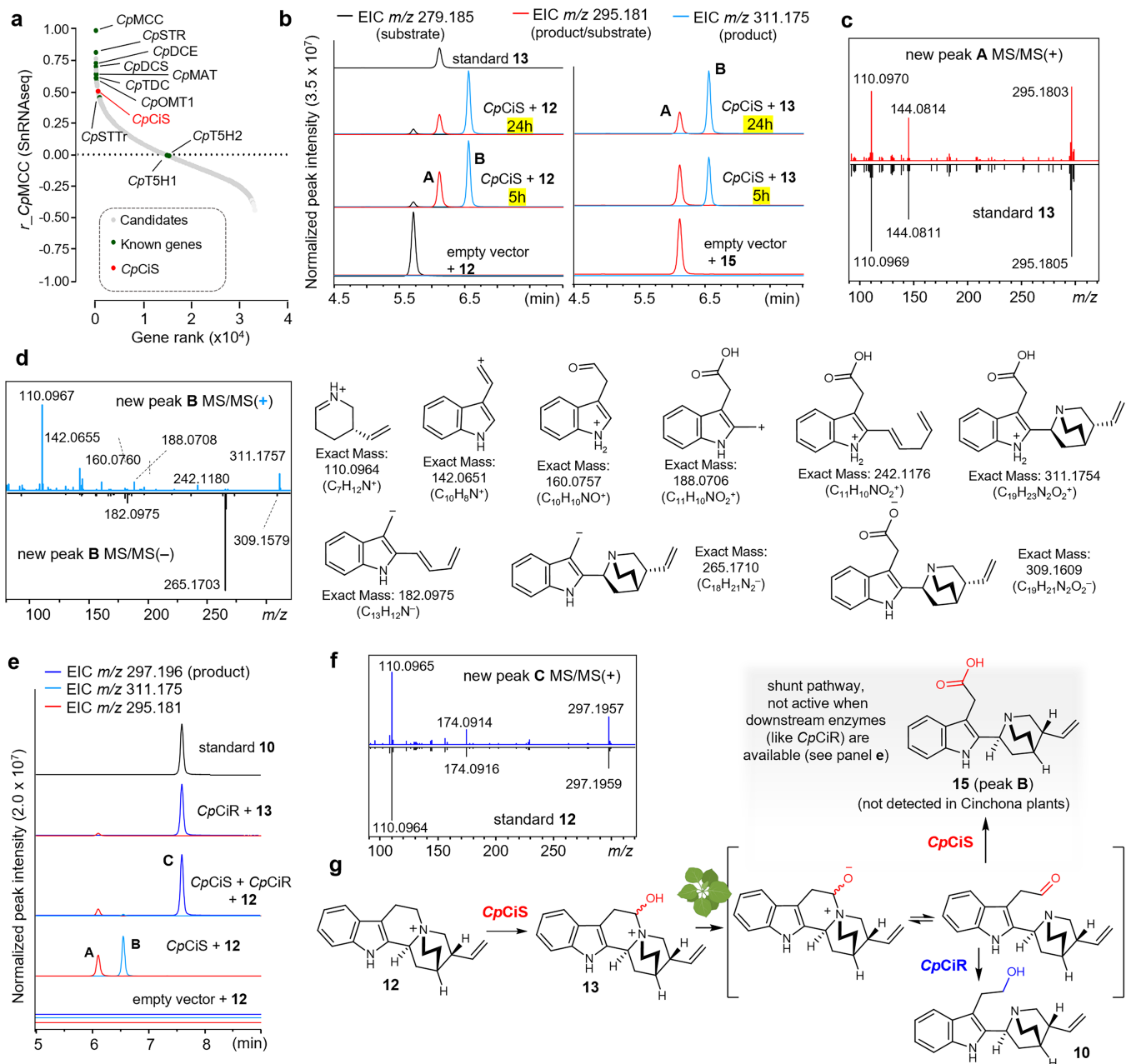
Reprints and permissions information is available at <http://www.nature.com/reprints>.



Extended Data Fig. 1 | Functional characterization of corynantheol reductases (*CpKR1-8*) and corynantheol malonyltransferase *CpMAT*.

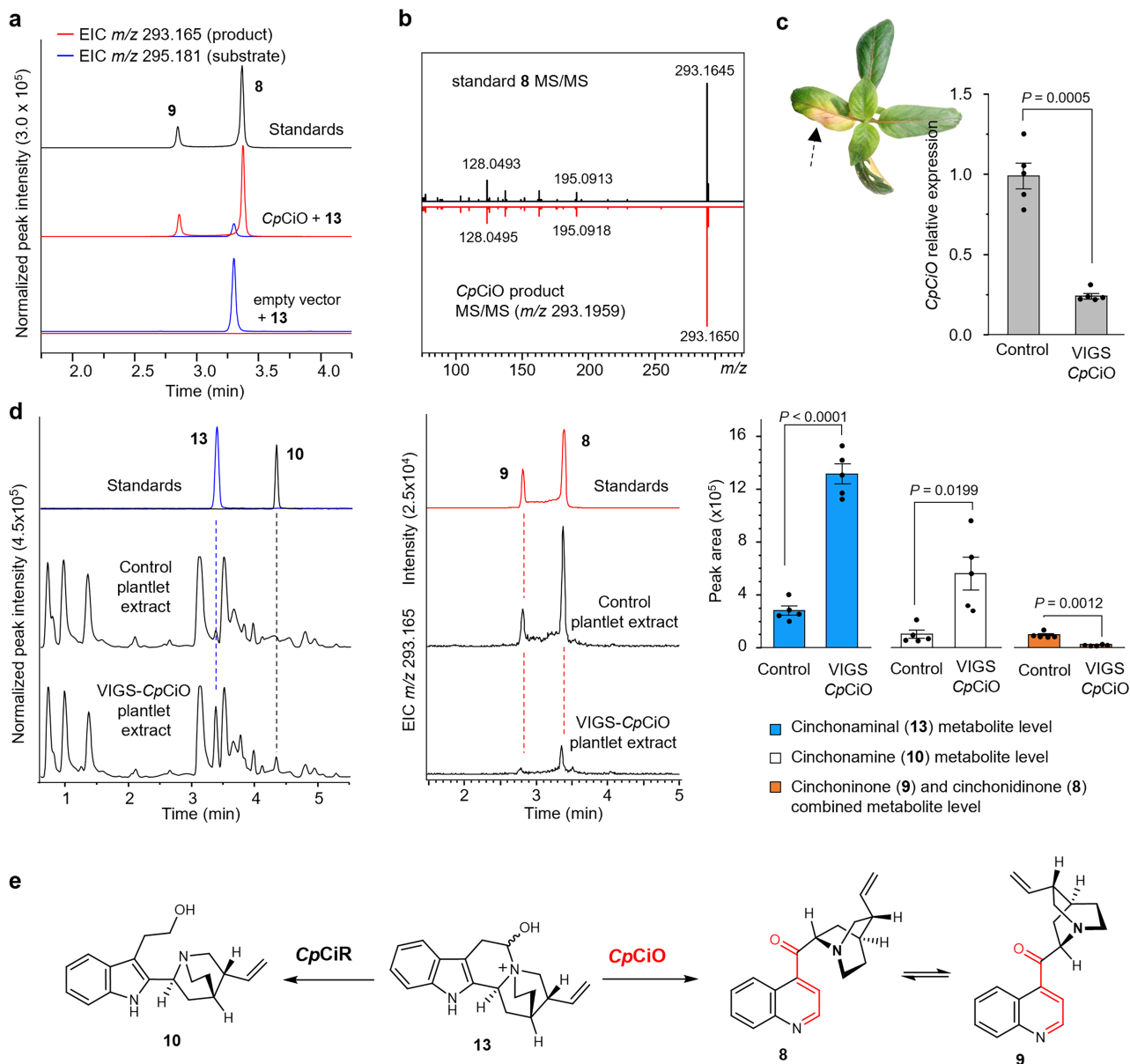
a. Reaction catalyzed by *CpKR1-8* with varied level of catalytic efficiency and co-expression with other pathway upstream genes *CpDCS*, *CpDE* and *CpSTR*. Data on *CpKR1-8* activity are mean \pm s.e.m. ($n = 3$). This experiment was repeated two times with similar results. **b.** Transient expression of *CpMAT* in *N. benthamiana* with co-infiltration of corynantheol (**11**). Extracted ion chromatograms for corynantheol (**11**) ($m/z 297.196 \pm 0.05$ Da $[M + H]^+$, green-highlighted) and malonyl-corynantheol (**14**) ($m/z 383.197 \pm 0.05$ Da $[M + H]^+$, red-highlighted). This experiment was repeated three times. Similar results were obtained in vitro using purified recombinant enzyme (see Supplementary Fig. 8). **c.** MS/MS (20 to 50 eV) spectrum of the *CpMAT* product and putative ion fragments of generated $m/z 383.1966$ $[M + H]^+$. **d.** Reaction catalyzed by *CpMAT*. **e.** VIGS-treated *C. pubescens* plantlets (transformed with a vector designed to silence magnesium chelatase subunit H (*CpMgChl*) encoding gene) and untreated plantlets. Leaf bleaching

(the yellow areas indicated by arrows) is the phenotypic characteristic of effective *CpMgChl* silencing. **f.** Relative expression of the gene encoding *CpMAT* in *C. pubescens* plantlets transformed with a vector designed to silence both *CpMAT* encoding gene and the marker gene *CpMgChl* (VIGS-*CpMAT*) and in control plantlets (transformed with a vector designed to silence only the marker gene *CpMgChl*) indicate the knockdown of *CpMAT*. **g.** Representative total ion chromatogram (TIC) of leaf tissue extracts from VIGS-*CpMAT*-transformed *C. pubescens* plantlets and control plantlets. Chromatograms for metabolites levels of the *CpMAT* knockdown tissue in comparison to controls are shown, corroborating the effective silencing of *CpMAT* encoding gene. Data in **f** and **g** are mean \pm s.e.m. ($n = 6$ biological replicates) and statistical analyses were performed using a two-sided, unpaired Welch's t-test. VIGS assays were repeated two times and one additional time with *C. pubescens* plantlets grown under various conditions with similar results. The icon in **d** was created in BioRender; Lombe, B. <https://biorender.com/8hz4n59> (2025).



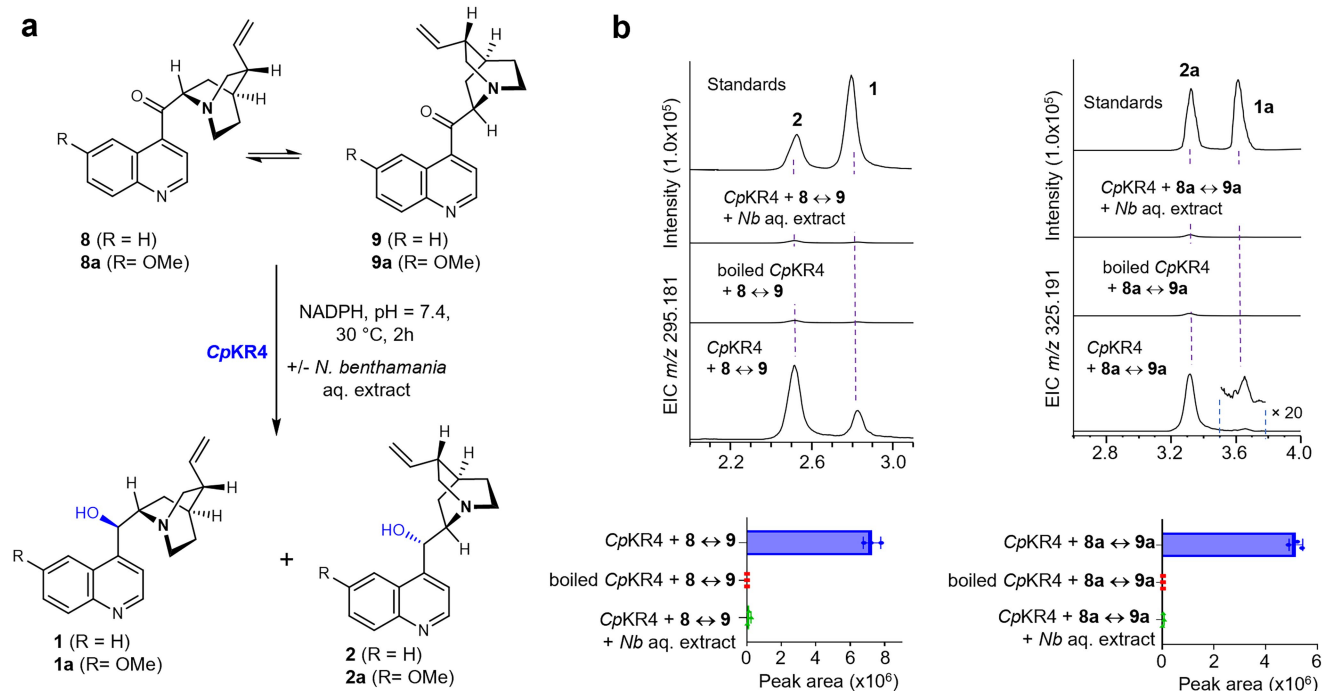
Extended Data Fig. 2 | Functional characterization of cinchonamine synthase (CpCiS) and cinchonamine reductase CpCiR. **a.** Ranking of hydroxylase (OGD and P450) gene candidates based on coexpression with CpMCC. **b.** Extracted ion chromatograms of the extract from the transient expression of CpCiS in *N. benthamiana* with infiltration of cinchonium (**12**, left) and cyclocinchonamine (**13**, right), which show that CpCiS converts **12** into **13** (peak A) and then transforms **13** into an overoxidized compound (peak B). This experiment was repeated five times with similar results. **c.** MS/MS (20 to 50 eV) spectra of the CpCiS product peak A and a standard cinchonamine (**13**). **d.** MS/MS (20 to 50 eV) spectra in positive (top) and negative (bottom)

mode of the CpCiS product peak B and putative fragments revealing the compound to be the carboxylic acid analog of cinchonamine, herein named cinchonamic acid (**15**). **e.** Extracted ion chromatograms of the extract from the transient expression of CpCiS and/or CpCiR in *N. benthamiana* with infiltration of cinchonium (**12**) or cyclocinchonamine (**13**), which show that CpCiR reduces **13** into cinchonamine (**10**) (peak C) and prevents an over oxidation of **13** by CpCiS. This experiment was repeated five times with similar results. **f.** MS/MS (20 to 50 eV) spectra of the CpCiR product peak C and a standard cinchonamine (**10**). **g.** Reaction catalyzed by CpCiS and CpCiR. The icon in **g** was created in BioRender; Lombe, B. <https://biorender.com/8hz4n59> (2025).



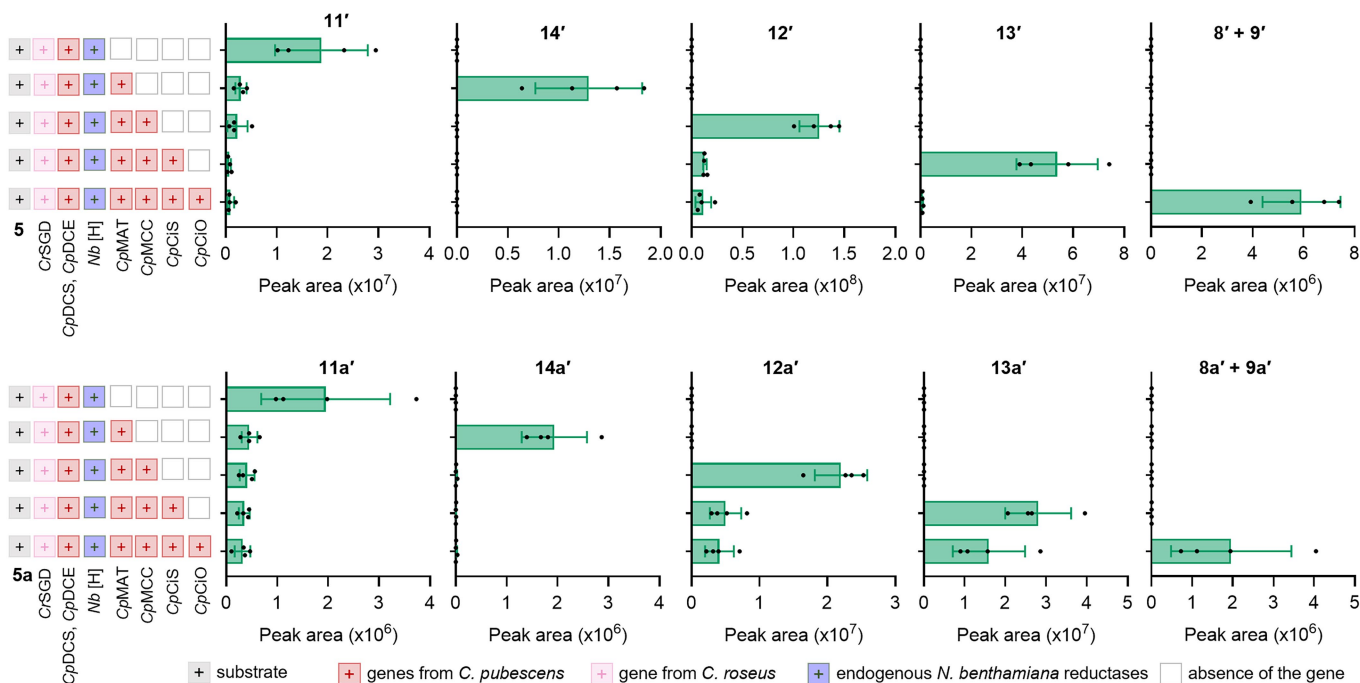
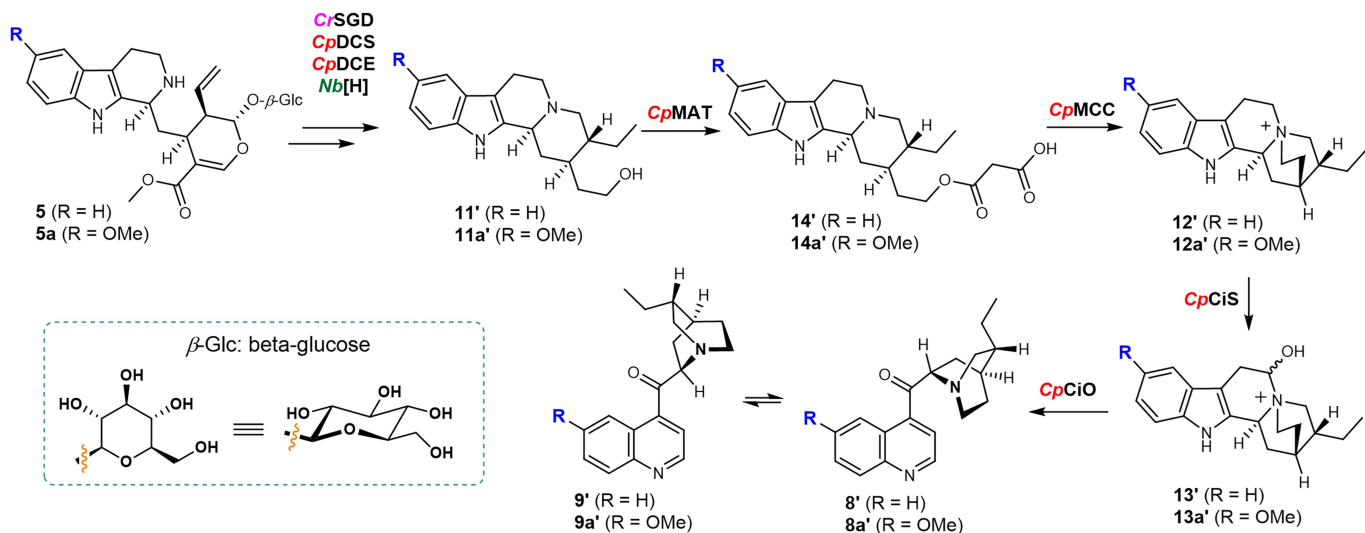
Extended Data Fig. 3 | Functional characterization of cinchonamine oxidase (CpCiO). **a.** Extracted ion chromatograms (EIC) of the extract from the transient expression of *CpCiS* in *N. benthamiana* with infiltration of cinchonaminol (**13**), showing that *CpCiO* converts **13** into quinoline compounds cinchonidinone (**8**) and cinchoninone (**9**), which exist in a tautomeric equilibrium. This experiment was repeated five times with similar results. **b.** MS/MS (20 to 50 eV) spectra of the *CpCiO* product and standard **8**. **c.** VIGS-treated *C. pubescens* plantlets transformed with a vector designed to silence *CpCiO* and the marker gene *CpMgChl*. The phenotypic characteristic resulting from *CpMgChl* silencing

(leaf bleaching) is indicated by an arrow and the relative expression of *CpCiO* is shown. **d.** Representative total ion chromatogram (TIC) of leaf tissue extracts from VIGS-*CpCiO*-transformed *Cinchona* plantlets and control plantlets, along with standards cinchonamine and cyclochinonaminol (**10** and **13**); EIC of cinchonidinone (**8**) and cinchoninone (**9**), and bar graphs for metabolite levels of the *CpCiO* knockdown tissue in comparison to controls are shown, corroborating the effective silencing of *CpCiO*. In **c** and **d**, the values represent mean \pm s.e.m. ($n = 5$ biological replicates) and statistical analyses were performed using a two-sided, unpaired Welch's *t*-test. **e.** Reaction catalyzed by *CpCiO*.



Extended Data Fig. 4 | Functional characterization of the keto-reductase *CpKR4*. **a.** *in vitro* reaction of *CpKR4* in the presence or absence of *N. benthamania* aqueous extract. **b.** EIC along with the LC-MS peak areas of reactions products, showing that *CpKR4* reduces the ketone-quinolines to the

Cinchona alkaloids, but this activity is inhibited by *N. benthamania* metabolites present in the aqueous extract. Another stereoisomer is also produced (Supplementary Fig. 31). Data are mean \pm s.d. ($n = 3$). This experiment was repeated three times with similar results.



Extended Data Fig. 5 | Step-by-step biosynthesis of Cinchona alkaloids in *N. benthamiana*. LC-MS peak areas of products detected in *N. benthamiana* following transient expression of the indicated biosynthetic enzymes and

incubation with either strictosidine (**5**) or 10-methoxystrictosidine (**5a**). Data are presented as mean \pm s.d. ($n = 4$ biological replicates).

Reporting Summary

Nature Portfolio wishes to improve the reproducibility of the work that we publish. This form provides structure for consistency and transparency in reporting. For further information on Nature Portfolio policies, see our [Editorial Policies](#) and the [Editorial Policy Checklist](#).

Statistics

For all statistical analyses, confirm that the following items are present in the figure legend, table legend, main text, or Methods section.

n/a Confirmed

- The exact sample size (n) for each experimental group/condition, given as a discrete number and unit of measurement
- A statement on whether measurements were taken from distinct samples or whether the same sample was measured repeatedly
- The statistical test(s) used AND whether they are one- or two-sided
Only common tests should be described solely by name; describe more complex techniques in the Methods section.
- A description of all covariates tested
- A description of any assumptions or corrections, such as tests of normality and adjustment for multiple comparisons
- A full description of the statistical parameters including central tendency (e.g. means) or other basic estimates (e.g. regression coefficient) AND variation (e.g. standard deviation) or associated estimates of uncertainty (e.g. confidence intervals)
- For null hypothesis testing, the test statistic (e.g. F , t , r) with confidence intervals, effect sizes, degrees of freedom and P value noted
Give P values as exact values whenever suitable.
- For Bayesian analysis, information on the choice of priors and Markov chain Monte Carlo settings
- For hierarchical and complex designs, identification of the appropriate level for tests and full reporting of outcomes
- Estimates of effect sizes (e.g. Cohen's d , Pearson's r), indicating how they were calculated

Our web collection on [statistics for biologists](#) contains articles on many of the points above.

Software and code

Policy information about [availability of computer code](#)

Data collection All presented data have been acquired using existing and routinely used softwares. These are mentioned in the respective parts in Methods. LC-MS data was collected with Bruker Compass qtofControl 5.2.109 / Hystar 5.1.5.1 or Thermo Scientific Xcalibur 4.7.69.37. NMR data were collected with Bruker TopSpin ver. 3.6.1. HPLC-UV data were acquired using Agilent OpenLAB CDS ChemStation 35900.

Data analysis All data analysis was done using routinely used softwares and online available bioinformatic platforms, as mentioned in the respective parts of the manuscript. LC-MS data were analysed using Bruker Compass DataAnalysis 6.1 and MetaboScape 2024b. LC-MS related graphs were prepared using OriginPro 9.6.0, GraphPad Prism 10.4.1, or SRplot v2025 (<https://www.bioinformatics.com.cn>), and were assembled in Microsoft PowerPoint 2024. Geneious Prime 2024 was used for primers design, sanger sequencing analysis, and translation of transcriptomes to proteomes. Normalization, visualization and clustering of RNA transcripts abundance were done using ClusterGVis (v0.1) and DESeq2 (v1.51.6). Phylogenetic trees were generated with MEGA11. Comparative transcriptomics analysis were done with OrthoVenn3 (<https://orthovenn3.bioinfotoolkits.net>). Protein structural models were predicted using AlphaFold 3 (<https://alphafoldserver.com>) and docking was done using AutoDock Vina on the SwissDock webserver (<https://www.swissdock.ch>) and visualised with PyMOL 2.5.3. Chemical structures were generated in ChemDraw Professional 23.1.12. Transcript reads were basecalled using Guppy (v6.3.2) and filtered with SeqKit (v0.16.1). The genome assembly was generated using Flye v2.9.1, Medaka v1.7.1 and Hapo-G v1.0. Genome annotation used RepeatMasker (v4.1.2-p1), RepeatModeler (v2.0.3), ProtExcluder (v1.2), Cutadapt (v2.10), HISAT2 (v2.1.0), Pychopper (v2.5.0), minimap2 (v2.17-r941), StringTie (v2.2.1), BRAKER2 (v2.1.6), PASA2 (v2.5.2), BLASTP (v2.12.0) and PfamScan (v1.6). Single nuclei transcriptomics data was processed with pipeseeker 3.1.3, STARsolo 2.7.10b, Seurat 4.3.0.1. Microsoft Excel 2014 and OriginPro 9.6.0 were used for statistical analysis.

For manuscripts utilizing custom algorithms or software that are central to the research but not yet described in published literature, software must be made available to editors and reviewers. We strongly encourage code deposition in a community repository (e.g. GitHub). See the Nature Portfolio [guidelines for submitting code & software](#) for further information.

Data

Policy information about [availability of data](#)

All manuscripts must include a [data availability statement](#). This statement should provide the following information, where applicable:

- Accession codes, unique identifiers, or web links for publicly available datasets
- A description of any restrictions on data availability
- For clinical datasets or third party data, please ensure that the statement adheres to our [policy](#)

Data supporting the findings of this work are available within this manuscript and its Supplementary Information files. Sequences of reported genes are included in Supplementary Information and are deposited in the National Center for Biotechnology (NCBI) GenBank under the following accession numbers: CpMAT (PX842829), CpMCC (PX842830), CpCiS (PX842831), CpCiR (PX842832), CpCiO (PX842833), CpSGD1 (PX842834), CpSGD2 (PX842835), CpSGD3 (PX842836), CpKR1 (PX842837), CpKR2 (PX842838), CpKR3 (PX842839), CpKR4 (PX842840), CpKR5 (PX842841), CpKR6 (PX842842), CpKR7 (PX842843), and CpKR8 (PX842844). *C. pubescens* bulk and single nuclei RNA-seq, ONT full length cDNA, and ONT genomic DNA reads are deposited in NCBI under BioProject PRJNA1347772. Raw reads from RNA-sequencing of *O. mungos* leaves have been deposited in NCBI (accession: PRJNA1413194). Bulk RNA-seq of *M. speciosa* from a previous study was downloaded from NCBI (accession PRJNA1244102) and the transcriptome of *A. thaliana* used is implemented and available in OrthoVenn3 (at <https://orthovenn3.bioinfotoolkits.net>). Proteomics data have been deposited to the ProteomeXchange Consortium (dataset identifier PXD068683). Source data are provided with this paper. The following databases were used for gene functional annotations TAIR (v10), Swiss-Prot Plant (2015_08) and PFAM (v35.0).

Research involving human participants, their data, or biological material

Policy information about studies with [human participants or human data](#). See also policy information about [sex, gender \(identity/presentation\), and sexual orientation](#) and [race, ethnicity and racism](#).

Reporting on sex and gender	Not applicable
Reporting on race, ethnicity, or other socially relevant groupings	Not applicable
Population characteristics	Not applicable
Recruitment	Not applicable
Ethics oversight	Not applicable

Note that full information on the approval of the study protocol must also be provided in the manuscript.

Field-specific reporting

Please select the one below that is the best fit for your research. If you are not sure, read the appropriate sections before making your selection.

- Life sciences Behavioural & social sciences Ecological, evolutionary & environmental sciences

For a reference copy of the document with all sections, see nature.com/documents/nr-reporting-summary-flat.pdf

Life sciences study design

All studies must disclose on these points even when the disclosure is negative.

Sample size	All experiments designed to probe the function of distinct enzymes were conducted with a sample size of at least three to ensure minimal statistical power analysis: <i>Nicotiana benthamiana</i> pathway reconstitution experiments were done on four independent biological replicates. In vitro assays were performed in three replicates. For VIGS studies, 5 to 6 biological replicates were used. Bulk RNA-seq of <i>Cinchona pubescens</i> was generated from five different plant tissues (three biological replicates each) for genes discovery, and from one replicate for <i>O. mungos</i> which is sufficient for cross-species transcriptomics comparison as no statistics were applied. Single-nuclei RNA-seq was performed on two biological replicates, which is sufficient for minimizing technical noise and identifying consistent cell-type-specific and gene-expression profiles, as also performed in several studies (e.g., <i>Nat. Commun.</i> 2025, 16, 3169; <i>Nat.</i> 2025, 643, 582; <i>Nat. Chem. Biol.</i> 2023, 19, 1031).
Data exclusions	No data was excluded from the analyses.
Replication	All experiments were repeated at least once and details about biological replicates are provided in the figure legends. Pathway reconstitution experiments were conducted on four biological replicates that correspond to four independent individual plants. All attempts of replication were successful. In vitro assays were performed as three technical replicates from the same enzyme purifications. Replications with different enzyme purifications were successful. VIGS experiments were successfully replicated twice, once with sterile plantlets and also using non-sterile 4-month-old plants grown on sand.
Randomization	For all LC-MS analyses, samples were loaded randomly on the mass spectrometer. To reduce variance, the order of injections into the LC-MS system was randomized, using the function RAND in Microsoft Excel. Plants and plantlets for gene expression profiling, gene heterologous expression, and VIGS assays were grown randomly in the growth chamber. For all the other experiments, randomization was not relevant.

Reporting for specific materials, systems and methods

We require information from authors about some types of materials, experimental systems and methods used in many studies. Here, indicate whether each material, system or method listed is relevant to your study. If you are not sure if a list item applies to your research, read the appropriate section before selecting a response.

Materials & experimental systems

n/a	Included in the study
<input checked="" type="checkbox"/>	<input type="checkbox"/> Antibodies
<input checked="" type="checkbox"/>	<input type="checkbox"/> Eukaryotic cell lines
<input checked="" type="checkbox"/>	<input type="checkbox"/> Palaeontology and archaeology
<input checked="" type="checkbox"/>	<input type="checkbox"/> Animals and other organisms
<input checked="" type="checkbox"/>	<input type="checkbox"/> Clinical data
<input checked="" type="checkbox"/>	<input type="checkbox"/> Dual use research of concern
<input type="checkbox"/>	<input checked="" type="checkbox"/> Plants

Methods

n/a	Included in the study
<input checked="" type="checkbox"/>	<input type="checkbox"/> ChIP-seq
<input checked="" type="checkbox"/>	<input type="checkbox"/> Flow cytometry
<input checked="" type="checkbox"/>	<input type="checkbox"/> MRI-based neuroimaging

Dual use research of concern

Policy information about [dual use research of concern](#)

Hazards

Could the accidental, deliberate or reckless misuse of agents or technologies generated in the work, or the application of information presented in the manuscript, pose a threat to:

No	Yes
<input checked="" type="checkbox"/>	<input type="checkbox"/> Public health
<input checked="" type="checkbox"/>	<input type="checkbox"/> National security
<input checked="" type="checkbox"/>	<input type="checkbox"/> Crops and/or livestock
<input checked="" type="checkbox"/>	<input type="checkbox"/> Ecosystems
<input checked="" type="checkbox"/>	<input type="checkbox"/> Any other significant area

Experiments of concern

Does the work involve any of these experiments of concern:

No	Yes
<input checked="" type="checkbox"/>	<input type="checkbox"/> Demonstrate how to render a vaccine ineffective
<input checked="" type="checkbox"/>	<input type="checkbox"/> Confer resistance to therapeutically useful antibiotics or antiviral agents
<input checked="" type="checkbox"/>	<input type="checkbox"/> Enhance the virulence of a pathogen or render a nonpathogen virulent
<input checked="" type="checkbox"/>	<input type="checkbox"/> Increase transmissibility of a pathogen
<input checked="" type="checkbox"/>	<input type="checkbox"/> Alter the host range of a pathogen
<input checked="" type="checkbox"/>	<input type="checkbox"/> Enable evasion of diagnostic/detection modalities
<input checked="" type="checkbox"/>	<input type="checkbox"/> Enable the weaponization of a biological agent or toxin
<input checked="" type="checkbox"/>	<input type="checkbox"/> Any other potentially harmful combination of experiments and agents

Seed stocks	N. benthamiana and A. thaliana seeds were obtained from seed stocks maintained by the greenhouse team at Max Planck Institute for Chemical Ecology, Jena. C. pubescens and Kratom seeds were obtained from Edinburgh botanical garden and the University of Florida, respectively. O. mungos was obtained as a plantlet from the Palmengarten botanical garden, as described in Plant Materials.
Novel plant genotypes	No plant stable transformation was performed in this study. Genes heterologous expression in N. benthamiana was carried out transiently through agroinfiltration of young leaves, as described in the methods paragraph "Transient gene expression in N. benthamiana". Virus-induced gene silencing in C. pubescens was also transient, as described in the methods section "Virus induced gene silencing (VIGS) in C. pubescens".
Authentication	Transient transformation of N. benthamiana through leaf agroinfiltration was done as described in the methods paragraph "Transient gene expression in N. benthamiana". Virus-induced gene silencing in C. pubescens was also transient as described in the Methods paragraph "Virus induced gene silencing (VIGS) in C. pubescens". No plant stable transformation was carried out.